A Survey for Large Image-Separation Lensed Quasars

Dan Maoz[1], Hans-Walter Rix[2,3], Avishay Gal-Yam[1], and Andrew Gould[4]

[1] School of Physics & Astronomy and Wise Observatory,

Tel-Aviv University, Tel-Aviv 69978, Israel.

dani@wise.tau.ac.il

[2] Steward Observatory, University of Arizona, Tucson, AZ 85721

rix@as.arizona.edu

[3] Alfred P. Sloan Fellow

[4] Department of Astronomy, Ohio State University, Columbus, OH 43210

gould@payne.mps.ohio-state.edu

ABSTRACT

The statistics of gravitationally lensed quasars with multiple images in the $0.1'' - 7''$ range have been measured in various surveys. Little is known, however, about lensed-quasar statistics at larger image separations, which probe masses on the scale of galaxy clusters. We extend the results of the *Hubble Space Telescope* (*HST*) Snapshot Survey for Lensed Quasars to the $7'' - 50''$ range for a sub-sample of 76 quasars that is free of known selection effects. Using a combination of multicolor photometry and spectroscopy, we show that none of the point sources in the entire field of view of the *HST* observations of these quasars are lensed images. Large-separation quasar lensing is therefore not common. We carry out a detailed calculation of the expected statistics of large-separation lensing for this quasar sample, incorporating realistic input for the mass profiles and mass function of galaxy clusters. We find that the observational null results are consistent with the expected effect of galaxy clusters, even if these have existed in their present form and number since $z \sim 2$ (and certainly if they were formed more recently). The rarity of large-separation lensed quasars can rule out some extreme scenarios, e.g. that the mass-function of clusters has been severely underestimated, or that large mass concentrations that are not associated with galaxies (i.e. "failed" clusters) are common. The rareness of cluster lensing also sets limits on the cosmological constant λ that are independent of limits derived from galaxy lensing. The lensing frequency

depends strongly on the central density of clusters. The lensing statistics of larger quasar samples (e.g. the Sloan Digital Sky Survey) can probe the structure, number, and evolution of clusters, as well as the geometry of space.

Subject headings: gravitational lensing – quasars: general – galaxies: clusters

submitted to *The Astrophysical Journal*: December 15, 1996

1. Introduction

The statistics of gravitational lensing can provide a powerful probe of the geometry and the mass content of the universe out to large redshifts (e.g. Refsdal 1964; Press & Gunn 1973). Turner, Ostriker, & Gott (1984) first explored lensing probabilities due to galaxies, and the resulting image separation distributions. The *Hubble Space Telescope* (*HST*) Snapshot Survey for lensed quasars (Bahcall et al. 1992; Maoz et al. 1992; 1993a; 1993b) was the first such large survey of a well-defined sample of 498 quasars. Exploiting the angular resolution of *HST*, it showed that about 1% of luminous quasars at $z > 1$ are gravitationally lensed into multiple images with separations in the $0.1'' - 7''$ range. Maoz & Rix (1993) used the Snapshot Survey results to demonstrate that early-type galaxies must have, on average, dark massive halos similar to those of spiral galaxies, and that the geometry of the Universe is not dominated by a cosmological constant λ, setting an upper limit of $\lambda < 0.7$. Ground-based surveys of 360 additional quasars and their analysis (see Kochanek 1996, and references therein) have confirmed these results. While the statistics of gravitationally lensed quasars with multiple images in the angular range expected due to galaxy lensing have been probed by the Snapshot and other surveys, little is known about lensed-quasar statistics at larger image separations, which probe masses on the scale of galaxy clusters. There are no confirmed cases of quasar splitting with separations above $7''$.[1]

Narayan & White (1988), Cen et al. (1994), Wambsganss et al. (1995), Kochanek (1995), and Flores & Primack (1996) have all compared large-scale structure formation models to the observed statistics of large-separation lensed quasars. However, the statistics utilized were the known lensed quasars in published catalogs, which are basically literature

[1] Saunders et al. (1997) recently suggested that PC1643+4631A&B ($198''$ separation) are images of a single quasar lensed by a massive $z \sim 1$ cluster, despite the fact that there is a small redshift difference in the spectra. Our results in the present work suggest that lensing with such image separations in highly unlikely.

compilations. As emphasized by Kochanek (1995), most quasars found in quasar surveys are near the faint detection limits of the surveys. The surveys will therefore generally not find faint lensed images of a given quasar, unless the two images are close in brightness. Kochanek (1995) estimates that that the completeness level of the catalogs, in terms of large-separation lenses, is only 20%. Furthermore, Gould, Bahcall, & Maoz (1993) have shown that quasar surveys using spectroscopic selection methods are biased against quasars having stars nearby in projection. Presumably, the same bias operates against neighboring lensed images, and would further select against inclusion of lensed quasars in the catalogs. There is therefore a possibility that large-separation lensing is more common than assumed, and that many such lensed quasars have been missed.

In the first part of this paper, we present the results of the first extensive survey for large-separation lensed quasars among known quasars. We use multi-color photometry and spectroscopy to test whether each of the point sources in the entire $70'' \times 70''$ field of view of the *HST* Planetary Camera (PC) exposures of 76 quasars in the original Snapshot Survey could be lensed images of the quasars. In the second part of the paper, we carry out a calculation of the expected lensing statistics for this particular sample and its observational parameters. The calculation follows closely that of Maoz & Rix (1993) and Rix et al. (1995) for small-separation lensing by galaxies, with galaxy clusters playing the previous role of galaxies. In addition to including effects such as magnification bias and observational detection limits, our calculation uses a realistic cluster mass profile that is motivated by N-body simulations (Navarro, Frenk, & White 1995, 1996, 1997) and is consistent with the observations of "radial arcs" in clusters (Bartelmann 1996). The choice of mass profile is important, since lensing calculations are sensitive to the presence of a core vs. a singular profile (e.g. Flores & Primack 1996).

2. Sample and Observations

In the *HST* Snapshot Survey for lensed quasars, 498 quasars were imaged with the Planetary Camera. The sample consisted of most of the quasars in the Véron-Cetty & Véron (1989) catalog with redshift $z > 1$, absolute magnitude $M_V < -25.5$ ($H_0 = 100$ km s^{-1} Mpc^{-1}, $q_0 = 0.5$), and galactic latitude $|b| > 10°$. (See Maoz et al. 1993b, for further details.) Gould, Bahcall, & Maoz (1993) catalogued all the point sources apearing in the PC exposure of each quasar to a typical limiting magnitude of $V \sim 21.3$ mag (see Gould, Bahcall, & Flynn 1996), and used them to study Galactic structure. Gould et al. (1993) found that quasars discovered by spectroscopic means (e.g. objective prisms) tended to "avoid" foreground stars out to separations of $40''$. The reason for this is unclear. The same

selection effect may operate on lensed images of the quasar, such that spectroscopically selected quasars are less likely to be lensed at separations above several arcseconds. Gould et al. (1993) defined an "unbiased" sample of 166 quasar fields in which the quasar was discovered by non-spectroscopic means (color-excess, radio, X-rays). For the present study, we have chosen from among the unbiased sample the 88 quasars in the anti-center Galactic hemisphere (i.e. $90^\circ < l < 270^\circ$, where l is Galactic longitude). By looking only at quasars in the anti-center hemisphere, we greatly reduce the number of stars that have to be checked to see if they are lensed images.

There are no point sources in the fields of 29 of the anti-center quasars, so these automatically pass the test for not being lensed (within the detection limits and the field of view probed by a given exposure). In nine additional quasar fields, the only other sources present are significantly brighter than the quasar. If they were lensed images of the quasars, they would have been identified as such by the original surveys. (This is not necessarily true of X-ray surveys, which may have poor angular resolution. However, the only objects around an X-ray selected quasar that were rejected based on this criterion are two $V \sim 12$ mag stars near the $V \sim 18$ mag quasar 0438−166.) We carried out V and I CCD photometry of the quasars and the point sources fainter than them in the remaining 50 quasar fields. Useful measurements were obtained for 38 of the fields. This leaves us with an observed sample of 76 quasars.[2] The 76 quasars and their parameters are listed in Table 1.

The V and I observations were made on 1993 March 4–9 at the Kitt Peak National Observatory (KPNO) and on 1993 September 5–10 at the Cerro Tololo Inter-American Observatory (CTIO). Both runs used Tektronix 1024-pixel CCDs at the Cassegrain focus of 0.9 m telescopes. Landolt (1992) standards were observed throughout the nights. Conditions were photometric, with a scatter of less than 0.03 mag around the fits to the Landolt magnitudes. The ground-based V and I magnitudes of each point source appearing in the *HST* exposures were measured using the Daophot point-source-function (PSF) fitting routine (Stetson 1987) within IRAF[3]. Errors were calculated by combining in quadrature the error in the photometric solution, as determined from its covariance matrix, the scatter

[2]A slight bias is introduced here, since isolated quasars are automatically included the sample, whereas some quasars surrounded with point sources are excluded. The bias could be corrected by eliminating from the sample a corresponding number (seven) of the isolated quasars. This would reduce the sample and the lensing predictions for it by 10%, not affecting any of our conclusions.

[3]IRAF (Image Reduction and Analysis Facility) is distributed by the National Optical Astronomy Observatories, which are operated by Aura, Inc., under cooperative agreement with the National Science Foundation.

around the photometric error, and the Daophot PSF-fitting error.

The V magnitude and $V-I$ color of each quasar and faint point source in the fields of the un-isolated quasars is listed in Table 2. The first line for each field gives the results for the quasar in the field, and the subsequent lines for the stars. Positions of the stars are given in Gould et al. (1993). The $V-I$ uncertainty listed in Table 2 does not include the absolute photometric calibration error, since this error cancels out in the *difference* between the $V-I$ color of a quasar and a star observed in the same CCD frame.

From a comparison of $V-I$ colors between each quasar and its neighboring objects, we can reject all stars in the fields of 26 quasars as candidate lensed images. The star near one quasar, 0024+22, can be rejected as a lensed image based on the absence of a radio counterpart (Condon et al. 1981), as described in Maoz et al. (1993a). The remaining 14 stars around 11 quasars have a color difference between star and quasar of $\Delta(V-I) < 0.3$ mag. Since such color differences among lensed images are possible due to differential reddening in the different light paths, these cases were kept for further testing. We measured B and V magnitudes for these remaining candidates on 1994 November 11 and 12 at the Wise Observatory 1m telescope with a Tektronix 1024×1024 back-illuminated CCD. The reduction and calibration was as for the KPNO and CTIO observations described above. The $B-V$ colors are given in Table 2.

If a $V-I$ color difference between lensed images is due to differential reddening, then the expected $B-V$ color difference among the images will be $\Delta(B-V) \approx 0.625\Delta(V-I)$ (Rieke & Lebofsky 1985). Based on $\Delta(B-V)$ significantly greater (after accounting for all the measurement errors) than expected from $\Delta(V-I)$ and reddening, we excluded eight of these stars, leaving six point sources in the fields of six quasars, each having both $V-I$ and $B-V$ colors similar to the quasar in their field. Spectra were obtained for these 6 sources at the Multiple-Mirror Telescope (MMT) on 1995, November 25–27, using a 1200 l/mm grating, covering 4500 Å to 6000 Å at 2 Å resolution. The spectra show that all six are foreground stars. They are marked as such in the right-hand column in Table 2.

We have thus demonstrated that none of the point sources detected in the PC field of view of 76 unbiased Snapshot Survey quasars in the anti-center hemisphere are lensed quasar images.

3. Calculation of Lensing by Clusters

3.1. Algorithm

We have carried out a calculation of the expected number and distribution in angular separation of lensed quasars due to the effects of intervening galaxy clusters. Our calculation follows closely that of Maoz & Rix (1993). Briefly, for a given observed quasar and a particular lens (i.e., a cylindrically-symmetric cluster of a particular redshift and mass) we find the "critical radius" inside which lensing into multiple images occurs. For every impact parameter inside this radius, we calculate the three image positions and their magnifications. We weight the image distribution for the particular lens according to the magnification bias, the cross section for lensing at that redshift, the number density of clusters of that mass, and the volume of space included in a redshift interval. We then integrate numerically the image distributions over grids in cluster mass and redshift (from $z = 0$ to z of the quasar), to obtain the probability that a given quasar in the sample is lensed, as a function of image separation. We weight this distribution for each quasar according to the detection efficiency as a function of image separation. These probability distributions are calculated for every quasar in the sample and added, to give the expected number, and distribution in image separation, of lensed quasars in the survey. We provide more details below, with emphasis on places where the calculation differs from Maoz & Rix (1993).

3.2. Cluster Mass Profile

To model the mass profile of galaxy clusters, we have used the radial mass density function

$$\rho(x) = \frac{\rho_s}{x(1+x)^2}, \tag{1}$$

where the radial coordinate, x, is in units of the scale radius r_s, $x \equiv r/r_s$. Navarro et al. (1995, 1996, 1997) have found that this mass profile describes well the dark-matter halos produced in cosmological N-body simulations for a variety of initial density fluctuation spectra. Note that at its center, the profile is singular, with $\rho \propto r^{-1}$. It is thus intermediate between the two types of mass profiles that have been considered in previous works on cluster lensing statitics, the singular isothermal sphere models, where $\rho \propto r^{-2}$, and models with a core, where ρ flattens to a constant at the cluster center. It is similar at small radii to the Hernquist profile, $\rho \propto r^{-1}(r+a)^{-3}$, considered by Flores & Primack (1996), but falls off more gently at large radii. Bartelmann (1996) has shown that the mass profile of equation 1 can produce radially distorted images of background sources, so-called "radial arcs", whose existence were previously thought to indicate cores in galaxy clusters. Flores & Primack (1996) have shown that, if clusters have large cores, the number of large-angle

splittings is greatly reduced, even in cosmological models with excessive large-scale structure (e.g. standard Cold Dark Matter [CDM]). They have argued that large-separation lensing is therefore not a sensitive probe of large-scale structure. Bartelmann's demonstration that clusters with a central density singularity can produce radial arcs renews that possibility that such clusters are efficient splitters of background quasars, and hence useful probes of large-scale structure and its evolution. In view of the results of Navarro et al. and Bartelmann, we consider equation 1 to be the one of the more realistic cluster mass profiles.

For our lensing calculations, we have used the expressions given by Bartelmann (1996) for the mass $m(x)$ enclosed within a cylinder of radius x. The bending angle of a light ray passing the cluster at impact parameter x, and hence the image positions and magnifications, are determined by $m(x)/x$ and its derivative (see, e.g., Maoz & Rix 1993). The mathematical details for the present case are provided in an Appendix.

From Figure 9 of Navarro et al. (1997) we estimate that that the scale length r_s depends on the cluster mass M as

$$r_s = 300 \left(\frac{M}{10^{15} M_\odot} \right)^\gamma h^{-1} \mathrm{kpc}, \tag{2}$$

where h is the Hubble constant in units of 100 km s^{-1} Mpc^{-1}. The index γ varies among cosmological models between $\gamma \sim 1/3$ (CDM) to $\gamma \sim 1$ (for a model with initial density fluctuation power spectrum of power-law form with index $n = 0$). When γ is large, low-mass clusters have dense central regions and can become efficient lenses.

3.3. Observational Detection Limits

As in Maoz & Rix (1993), we have incorporated the detection limits for multiple images for each quasar into the calculation. In Maoz & Rix (1993), the detection limits included the angular resolution limit for detection of images with a given brightness ratio, and the flux limit of the exposure. In the present work, we have also included the incompleteness of the survey at large angular separations due to the positioning of the quasar on the PC field of view. For technical reasons, the quasar was generally not in the center of the PC field of view. The angular range from $0'' - 70''$ was therefore covered with a varying degree of completeness for each angle and each quasar. For every quasar, the lensing probability distribution at angle θ was scaled by a factor equal to the fraction of a circle, of radius $2\pi\theta$ with center at the quasar position, that is within the PC field of view. The position of each quasar on the PC is given in Table 1. See Maoz et al. (1993) for more details on the PC observations. The effect of this angular selection function on the completeness of the survey is examined in §4.

3.4. Magnification Bias

The magnification bias is the over-representation of lensed quasars in a flux-limited quasar sample due to the facts that lensing increases the apparent brightness of a quasar and that there are more faint quasars than bright ones. The magnification bias is calculated as in Maoz & Rix (1993), with the probability $P(A)$ for amplification by a factor A calculated for the cluster lenses under consideration here. We have updated the slopes of the quasar luminosity function to $\alpha = -1.3 \pm 0.2$, $\beta = -3.87 \pm 0.15$, the absolute magnitude of the break in the local luminosity function to $M^*_{Q0} = -20.87 \pm 0.25$ and the luminosity evolution power-law index to $k_L = 3.2 \pm 0.1$, according to the results of Boyle et al. (1990).

3.5. Cluster Mass Function and Evolution

To represent the number density of clusters of a given mass, we have used the observational results of Bahcall & Cen (1993), rather than the theoretical large-scale structure predictions used by previous studies of large-separation lensing. Bahcall & Cen find that, for groups and clusters of galaxies with mass M between 10^{13} and $10^{15} M_\odot$, the mass function can be represented analytically by $n(> M) = 4 \times 10^{-5} (M/M^*)^{-1} \exp(-M/M^*) h^3$ Mpc^{-3}. Here $M^* = (1.8 \pm 0.3) \times 10^{14} h^{-1} M_\odot$,and M is the mass within a $1.5 h^{-1}$ Mpc radius sphere around the cluster center.

Bahcall & Cen also show that the extrapolation of this function to $10^{12} M_\odot$ has a value similar to the space density of "noncluster" L^* *galaxies*, and note that this continuity is expected from general theoretical expectations (e.g. Press & Schechter 1974). Since the observed galaxy luminosity function actually has an exponential cutoff at $L*$, the implication would be that dark halos form at all masses, but when the mass is above $10^{12} M_\odot$, a group or a cluster will form in it, rather than a galaxy. In practice, it is unknown whether or not dark halos in the $10^{12} - 10^{13} M_\odot$ range exist. Since, as will turn out, halos in this mass range can be important for large separation lensing, we will allow for two possibilities: that the cluster mass function can be extrapolated down to $10^{12} M_\odot$, as in Bahcall & Cen, or that there is a lower cutoff to the mass of clusters at $10^{13} M_\odot$ (i.e. a gap in the halo mass function, contrary to Press-Schechter theory). We will further examine the consequences of such a gap in §4.

The derivative of $n(> M)$ with respect to M gives $n_0(M)$, the local ($z = 0$) space density of clusters of mass M to $M + dM$. As a first approximation, we have assumed that the number of clusters per co-moving volume element does not evolve between $z = 0$ and the redshift of the quasar (typically $z \sim 2$), i.e. the number density at z

is $n(z) = n_0(1+z)^3$. Flores & Primack (1996) show that the no-evolution assumption is a reasonable approximation to the numerical CDM calculation of Cen et al. (1994), and occurs because a cluster-sized perturbation is already virialized inside a radius of $200(v/1000 \text{ km s}^{-1})h^{-1}$ kpc by $z = 3$. It is the inner parts of the cluster which determine the lensing statistics. In non-CDM models, clusters may form more recently, and one would expect that at higher z there are fewer clusters and/or the mass in clusters is less concentrated. However, we find that even with the simplistic assumption of no evolution, the expected number of large-separation lensed quasars in the survey is generally < 1, and hence consistent with the observed null result. Clearly, incorporation of recent cluster formation would further lower the prediction. More details on the results and their dependence on the input parameters are given below.

4. Results and Discussion

We have calculated the number of lensed quasars we expect to detect in our sample as a function of image separation for a variety of combinations of the input parameters of clusters. Figure 1 shows the expected distribution for a particular choice of parameters. Also shown is the distribution that would result if the angular selection function resulting from the positioning of the quasar on the PC did not exist. We see that the angular selection function does not seriously impair our ability to detect lensed quasars, and has some effect only at the largest ($> 30''$) separations. The total number of expected lensed quasars above $7''$ separation in this particular model is 0.032 (0.041 without the angular selection function), consistent with our null result.

Although the clusters produce lensed quasars with separations smaller than $7''$ too, comparison to the observations in the $0'' - 7''$ range is complicated because lensing with such separations is produced by galaxy lenses as well. A case in point is the lensed quasar 0957+561, with $6.1''$ image separation. It was not observed with *HST* because it was previosly known to be lensed but, in principle, it is part of the Snapshot sample (see Maoz et al. 1992). Since it is radio-discovered and in the anti-center hemisphere, it would be included in the present sample as well. However, a cluster and a galaxy both play a significant role in lensing this quasar. It would therefore be unclear whether or not it counts as one detection when comparing to the predictions of lensing by clusters. By comparing models and observations only for separations $> 7''$, we restrict ourselves to lensing by clusters alone.

A free parameter in our calculation is γ, the power-law index relating the scale radius r_s to the total cluster mass (eq. 2). Navarro et al. (1997) predict that γ varies

between cosmological models in the range of 1/3 to 1. Among the input parameters, the total number of lensed quasars is, by far, most sensitive to γ. A large γ gives low- and intermediate-mass clusters a large central density, turning them into efficient lenses. Figure 2 shows the lensing distribution on a logarithmic scale for various values of γ. The models with $\gamma \lesssim 0.7$ produce $<< 1$ lensed quasars in our sample. These models are therefore consistent with our observed null result, even if the other input parameters, such as the number density of clusters or the mass of an M^* cluster have both been underestimated by an order of magnitude.

On the other hand, models with $\gamma \sim 1$ produce about one expected lens for the "standard" input parameters (the Bahcall & Cen 1993 mass function and an Einstein-de Sitter $\Omega = 1$ cosmology). Models predicting 3 (4.5) or more lenses can be rejected at $> 95\%$ ($> 99\%$) confidence based on Poisson statistics. Factors of a few in the predicted number of lenses can result from mild changes in the parameters of the mass function (which is empirically not well constrained) or the cosmology (e.g., lowering Ω, or introducing a cosmological constant λ will raise the prediction). Some models with high γ and various combinations of the other parameters can therefore be rejected.

Figure 3 shows the dependence of the lensing distribution on M^*, the exponential upper mass cutoff in the cluster mass function. For low γ, the total number and the mean image separation of lensed quasars both increase with M^*. At higher γ (not shown), the total number of lensed quasars is insensitive to M^*, and only the centroid of the distribution shifts slowly with M^*. This occurs because, for large γ, the more massive clusters that are introduced by raising M^* have large scale lengths, and so do not lens effectively.

The parameter plane of γ and M^* is shown in Figure 4, which gives the total number of predicted lensed quasars with $> 7''$ separation for combinations of these parameters. $\Omega = 1$ and the Bahcall & Cen (1993) value of $n(M^*)$, the number density of M^*-mass clusters, are assumed. Increasing $n(M^*)$ would increase the number of lensed quasars by the same proportion. We see that, if γ is large, the number density of clusters cannot be much above the Bahcall & Cen (1993) estimate, or some lensed quasars would have been found in the survey. A great advantage of gravitational lensing is that it probes mass, rather than light. The above result therefore also shows that, unless γ is small, there cannot be a large population of "failed clusters", i.e. dark halos not containing clusters of galaxies. The predicted number of lensed quasars approximately doubles when going from a flat $\Omega = 1$ to an open $\Omega = 0$ model. Low-density open models with $\gamma \sim 1$ predict more than 3 lenses, so are inconsistent with the data.

Because dense, low-mass clusters can be efficient lenses, introducing a lower mass cutoff at $10^{13} M_\odot$ in the cluster mass function (see §3.5) greatly reduces the lensing prediction.

For example, in a $\gamma = 0.8$ model, the expected lensing distribution decreases by a factor of ~ 30 below $10''$, and by a factor of ~ 4 above $10''$, so the total expected number of lensed quasars decreases by about a factor of 15. For $\gamma = 0.67$ (i.e., low-mass clusters are not so dense) the distribution decreases by a factor of ~ 2 below $10''$, but is unchanged above $10''$.

Finally, high-γ models in a flat Universe dominated by a cosmological constant can also be ruled out. This is shown in Figure 5, displaying the $\lambda - \gamma$ plane. For example, a model with $\gamma = 1$ and $\lambda = 0.7$ produces over 5 lensed quasars in our sample. This limit on λ is independent of the limits that have been derived based on small-separation quasar lensing by galaxies (Fukugita & Turner 1990; Maoz & Rix 1993; Kochanek 1996). Fukugita & Peebles (1993) and Malhotra, Rhoads, & Turner (1997) have suggested that small-separation lensing statistics can be reconciled with a λ-dominated Universe by invoking dust in the lensing galaxies. The excess number of lensed quasars would then be hidden by extinction. This argument is not applicable to lensing by clusters. Maoz (1995) has shown that rich clusters do not significantly redden quasars that are behind them. A similar demonstration has been made for poorer clusters by Williams & Hawkins (1996). Conversely, if the dependence of cluster scale length on cluster mass is weak (i.e. if γ is small), or if there is a significant decrease in the number of clusters between now and $z \sim 2$, or if there is a gap in the halo mass function between masses of $\sim 10^{12} - 10^{13} M_\odot$, a λ-dominated Universe is allowed by the present large-separation lensing statistics.

Due to the smallness of this first large-separation sample, we have limited the range of models we have examined, and avoided complications such as evolution in cluster number and structure. Upcoming surveys, such as the Sloan Digital Sky Survey, will detect and test orders of magnitude more quasars for lensing by galaxies and by clusters. If γ is small, we predict that even these surveys will find no examples of large-separation lensed quasars. If, on the other hand, clusters have dense centers, many such lenses will be found. Their detailed statistics can then serve as a valuable probe of the structure, number, and evolution of galaxy clusters, and of the geometry of the Universe.

We thank J. Wambsganss for suggesting this project.

A. The Lensing Equation for Clusters

A light ray passing with an impact parameter b from the center of a cylindrically symmetric mass distribution is bent by an angle (e.g. Weinberg 1972)

$$\alpha = \frac{4GM(< b)}{c^2 b}, \tag{A1}$$

where $M(< b)$ is the total mass that is projected inside of b. The lensing equation, relating the angle θ_I between the lens and the projected image to the angle θ_S between the source and the lens, is

$$\theta_S = \frac{D_{LS}}{D_{OS}}\alpha(\theta_I) - \theta_I, \tag{A2}$$

where D_{LS} and D_{OS} are the angular diameter distances between the lens and the source and between the observer and the source, respectively. The condition for gravitationally lensing a source into multiple images is that the source be projected on the sky within an angle $\theta < \theta_{cr}$ of the lens,

$$\theta_{cr} = \frac{D_{LS}}{D_{OS}}\alpha(\theta_1) - \theta_1. \tag{A3}$$

where θ_1 is defined by

$$\frac{D_{LS}}{D_{OS}}\frac{d\alpha}{d\theta}\Big|_{\theta=\theta_1} = 1. \tag{A4}$$

For a lensing cluster with surface density profile $\Sigma(r)$ and scale radius r_s, Equation (A1) can be rewritten as:

$$\alpha = \frac{4GM_{1.5}}{c^2 r_s} f(x), \tag{A5}$$

where $M_{1.5}$ is the mass enclosed within $1.5h^{-1}$ Mpc, the dimensionless function $f(x)$ is defined as

$$f(x) \equiv \frac{1}{x}\frac{\int_0^x \Sigma(r) r dr}{\int_0^{1.5\mathrm{Mpc}} \Sigma(r) r dr} = \frac{1}{x}\frac{g(x)}{g(1.5\mathrm{Mpc}/r_s)}, \tag{A6}$$

and

$$x \equiv \frac{b}{r_s}. \tag{A7}$$

$g(x)$ for the mass profile of equation 1 is given by Bartelmann (1996) as

$$g(x) = \ln\frac{x}{2} + \begin{cases} \frac{2}{\sqrt{x^2-1}} \arctan\sqrt{\frac{x-1}{x+1}} & (x>1) \\ \frac{2}{\sqrt{1-x^2}} \operatorname{arctanh}\sqrt{\frac{1-x}{1+x}} & (x<1) \\ 1 & (x=1) \end{cases}. \tag{A8}$$

Combining equations (A3) and (A5), we can write the critical radius for lensing as:

$$r_{cr} = r_s\left(\frac{\Sigma_{av}}{\Sigma_{cr}} f(x_1) - x_1\right). \tag{A9}$$

Here $\Sigma_{av} \equiv M_{1.5}/\pi r_s^2$, Σ_{cr} is the critical surface mass density, defined as

$$\Sigma_{cr} \equiv \frac{c^2}{4\pi G}\frac{D_{OS}}{D_{OL}D_{LS}}, \tag{A10}$$

where D_{OL} is the angular diameter distance from the observer to the lens, and $x_1 = D_{OL}\theta_1/r_s$, so that, from equation (A4),

$$\left.\frac{df}{dx}\right|_{x_1} = \frac{\Sigma_{cr}}{\Sigma_{av}}. \tag{A11}$$

We show in Figure A1 the functions $g(x)/x$ and $d(g(x)/x)/dx$. Determining the critical radius for a cluster of given mass involves solving numerically equation (A11) for x_1 and substituting x_1 into equation (A9).

REFERENCES

Bahcall, J.N., Maoz, D., Doxsey, R., Schneider, D.P., Bahcall, N.A., Lahav, O. & Yanny, B. 1992, ApJ, 387, 56

Bahcall, N.A., & Cen, R. 1993, ApJ, 407, L49

Bartelmann, M. 1996, A&A, in press

Boyle, B.J., Fong, R., Shanks, T., & Peterson B.A. 1990, MNRAS, 243, 1

Cen, R., Gott, J.R., Ostriker, J.P., & Turner, E.L. 1994, ApJ, 423, 1

Condon, J.J., O'Dell, S.L., Puschell, J.J., & Stein, W.A. 1981, ApJ, 246, 624

Flores, R. A., & Primack, J. R. 1996, ApJ, 457, L5

Fukugita, M. & Turner, E.L. 1991, MNRAS, 253, 99

Fukugita, M., and Peebles, P.J.E. 1993, preprint, astro-ph/9305002

Gould, A., Bahcall, J.N., and Maoz, D. 1993, ApJS, 88, 53

Gould, A., Bahcall, J.N., Maoz, D., & Yanny, B. 1995, ApJ, 441, 200

Gould, A., Bahcall, J.N., & Flynn, C. 1996, ApJ, 465, 759

Kochanek, C.S. 1995, ApJ, 445, 559

Kochanek, C.S. 1996, ApJ, 466, 638

Landolt, A.U. 1992, AJ, 104, 372

Malhotra, S., Rhoads, J.E., & Turner, E.L. 1997, MNRAS, submitted, astro-ph/9610233

Maoz, D. 1995, ApJ, 455, L115

Maoz, D., Bahcall, J.N., Schneider, D.P., Doxsey, R., Bahcall, N.A., Lahav, O. & Yanny, B. 1992, ApJ, 394, 51

Maoz, D., Bahcall, J.N., Schneider, D.P., Doxsey, R., Bahcall, N.A., Lahav, O. & Yanny, B. 1993a, ApJ, 402, 69

Maoz, D., Bahcall, J.N., Schneider, D.P., Bahcall, N.A., Djorgovski, S., Doxsey, R., Gould, A., Kirhakos, S., Meylan, G., & Yanny, B. 1993b, ApJ, 409, 28

Maoz, D. & Rix, H.-W. 1993, ApJ, 416, 425

Narayan, R., & White, S.D.M. 1988, MNRAS, 231, 97p

Navarro, J., Frenk, C.S., & White, S.D.M. 1995, MNRAS, 275, 720

Navarro, J., Frenk, C.S., & White, S.D.M. 1996, ApJ, 462, 563

Navarro, J., Frenk, C.S., & White, S.D.M. 1997, ApJ, submitted, astro-ph/9611107

Press, W.H. & Schechter, P.L. 1974, ApJ, 187, 425

Rieke, G.H., & Lebofsky, M.J. 1985, ApJ, 288, 618

Rix, H.-W., Maoz, D., Turner, E.L., & Fukugita, M. 1994, ApJ, 435, 49

Saunders, R., et al. 1997, ApJL, in press, astro-ph/9611219

Stetson, P.B. 1987, PASP, 99, 191

Turner, E.L., Ostriker, J.P., & Gott, J.R. 1984, ApJ, 284, 1

Véron-Cetty, M.P., & Véron, P. 1989, "A Catalogue of Quasars and Active Nuclei (5th Edition)" (Munich:ESO)

Wambsganss, J., Cen, R., Ostriker, J.P., & Turner, E.L. 1995, Science 268, 274

Weinberg, S. 1972, *Gravitation and Cosmology*, (New York: Wiley)

Williams, L.L.R., & Hawkins, M.R.S. 1996, MNRAS,

Table 1. Unbiased Anticenter Snapshot Quasar Sample

Quasar	Other Name[1]	Sel[2]	l^{II}	b^{II}	V^3	z	$-M_V^4$	PC position[5]
0004+171		R	108.03	−44.11	18.7	2.89	25.9	6(550,595)
0024+22		C	115.66	−39.83	17.0	1.11	25.6	8(174,629)
0033+0951	4C09.01	R	116.84	−52.56	17.7	1.92	26.0	6(304,308)
0058+0155	PHL938	C	127.75	−60.59	17.1	1.93	26.6	7(190,552)
0100−270		R	205.78	−87.41	18.1	1.60	25.2	8(186,149)
0109+17		R	129.76	−44.70	18.7	2.15	25.3	7(184,211)
0119−04		R	142.30	−66.06	17.0	1.95	26.8	6(285,310)
0122−00		R	141.16	−61.76	16.6	1.07	25.9	8(628,073)
0132+20		C	136.45	−40.96	17.9	1.78	25.7	6(343,318)
0136+176		R	194.15	−78.45	18.7	2.73	25.7	6(389,352)
0136−231		R	138.85	−43.49	17.8	1.89	25.9	6(121,278)
0151+0448	PHL1222	C	150.40	−54.46	17.9	1.91	25.8	6(152,219)
0215+165		R	151.18	−41.27	17.5	1.90	26.2	6(251,344)
0220−142		R	185.79	−65.00	18.8	2.43	25.4	6(239,223)
0225−014		R	168.86	−55.26	18.6	2.03	25.2	7(266,300)
0226−038		R	171.90	−56.93	17.2	2.06	26.7	6(242,259)
0229+13		R	157.09	−42.74	17.9	2.07	26.0	6(258,258)
0232−04		R	174.46	−56.16	16.3	1.43	26.8	6(246,225)
0244−128		R	190.42	−59.32	18.4	2.2	25.6	6(232,260)
0256−005		R	177.19	−49.23	17.5	1.99	26.3	8(362,061)
0302−223		X	211.08	−59.39	16.9	1.41	26.2	6(167,150)
0329−255		R	219.43	−54.30	17.8	2.69	26.6	6(250,214)
0335−336		X	233.40	−53.87	18.5	2.27	25.6	6(169,258)
0347−241		R	218.73	−49.98	17.1	1.88	26.6	8(734,115)
0355−48		R	256.16	−48.45	16.6	1.01	25.8	6(240,261)
0402−362		R	237.74	−48.48	16.9	1.42	26.2	6(220,241)
0438−166		X	214.14	−36.25	17.9	1.96	25.9	6(253,237)
0438−43		R	248.41	−41.57	19.5	2.85	25.0	6(248,258)
0448−392		R	242.77	−39.61	16.7	1.29	26.2	6(227,237)
0451−28		R	229.02	−37.02	18.2	2.56	26.1	6(243,262)
0636+68		R	147.17	24.15	16.6	3.17	28.2	6(105,133)
0642−349		R	244.29	−16.49	18.0	2.17	26.0	7(262,160)
0731+65		R	151.00	29.12	18.2	3.03	26.5	6(246,245)
0759+341		R	187.12	28.74	18.5	2.44	25.7	6(066,344)
0804+4959	OJ508	R	169.16	32.56	18.3	1.43	24.8	6(422,265)
0808+28		R	193.47	29.13	18.3	1.91	25.4	6(252,264)
0812+33A		R	188.89	31.10	19.2	2.42	25.0	6(271,226)
0827+24		R	200.02	31.88	17.5	2.06	26.4	6(256,226)
0830+115		R	213.99	27.71	18.0	2.97	26.6	6(236,260)
0831+101		R	215.61	27.42	19.6	1.76	23.9	8(378,109)
0836+1932	4C19.31	R	206.13	32.10	17.6	1.69	25.9	8(633,180)
0838+4536	US1498	C	174.94	37.97	17.5	1.41	25.6	6(052,202)
0843+1339	4C13.39	R	213.25	31.36	17.5	1.88	26.2	6(047,276)
0848+1533	LB8755	C	211.77	33.24	17.8	2.01	26.0	6(265,237)
0848+1623	LB8775	C	210.93	33.74	17.6	1.93	26.1	6(250,227)
0854+1907	LB8956	C	208.45	36.00	18.0	1.89	25.7	6(240,251)
0856+124		R	216.18	33.93	19.4	1.76	24.1	8(293,096)
0903+175		X	211.22	37.49	18.0	2.77	26.5	6(255,198)
0907+381		R	185.04	42.97	17.6	2.16	26.4	6(248,271)
0932+367		R	187.39	47.80	18.4	2.84	26.1	6(281,176)
0945+114		R	224.00	44.12	18.9	2.14	25.0	6(079,300)
0945+4337	US987	C	176.79	49.90	18.2	1.89	25.5	6(138,087)

Table 1—Continued

Quasar	Other Name[1]	Sel[2]	l^{II}	b^{II}	V^3	z	$-M_V^4$	PC position[5]
0946+301		C	197.83	50.24	16.2	1.22	26.6	6(297,288)
0955+4739	OK492	R	170.06	50.73	18.7	1.87	25.0	6(255,252)
1008+133		C	225.40	50.05	16.3	1.29	26.6	6(217,353)
1011+091		X	231.51	48.54	17.7	2.26	26.4	6(249,223)
1038+065	4C06.41	R	241.11	52.65	16.6	1.27	26.3	6(243,264)
1038+528		R	157.50	54.97	18.6	2.30	25.5	7(615,291)
1045+60	4C60.15	R	146.72	50.93	18.7	1.72	24.8	8(074,330)
1137+30	US2778	C	197.29	74.12	16.7	1.57	26.6	7(265,653)
1139+2833	US2828	C	204.60	74.70	17.3	1.61	26.1	6(470,667)
1148+38		R	167.15	73.11	17.2	1.30	25.7	6(232,251)
1206+459		C	144.63	69.62	15.5	1.15	27.1	6(237,228)
1211+33		R	173.89	79.92	17.6	1.60	25.7	6(247,243)
1215+33		R	171.72	80.56	18.1	2.60	26.2	6(180,177)
1215+6423	4C64.15	R	128.99	52.61	18.1	1.29	24.8	7(232,122)
1246+3746	BSO1	C	125.76	79.61	17.2	1.24	25.6	5(652,231)
1248+401		C	123.48	77.27	16.1	1.03	26.3	6(513,361)
1257+34	B201	C	109.54	82.52	16.7	1.37	26.3	6(237,254)
1259+3427	BSO6	C	105.93	82.60	18.0	1.95	25.8	8(283,078)
1309+3402	BSO8	C	91.00	82.06	17.7	1.75	25.8	7(289,092)
1323+6530	4C65.15	R	117.22	51.50	17.5	1.62	25.9	6(393,134)
1356+5806	4C58.29	R	106.58	57.09	17.2	1.37	25.8	6(266,344)
2251+24		R	91.71	−30.91	18.5	2.33	25.6	7(345,288)
2345+061		R	96.24	−53.16	18.1	1.54	25.2	6(251,256)
2353+154		R	103.82	−45.11	18.3	1.80	25.3	6(039,303)

Note. —

[1] Listed for objects for which Véron-Cetty and Véron (1989) give a name that does not include the coordinates.

[2] Quasar discovery method: R-radio; C-color; X-x-ray.

[3] V magnitude determined from the HST exposure, accurate to $\approx \pm 0.1$ magnitudes.

[4] Absolute V magnitude, assuming $H_0 = 100$ km s^{-1} Mpc^{-1}, $q_0 = 0.5$.

[5] Planetary Camera (PC) CCD number (5 through 8) and pixel coordinate with the origin at the PC apex.

Table 2. Quasar Fields with Stars

QSO Field	V	σ	$V-I$	σ	$B-V$	σ	Comments
0004+17	18.607	0.019	0.611	0.022			
	20.396	0.049	1.549	0.061			
	19.755	0.029	1.692	0.033			
0024+22	16.583	0.015	0.509	0.014			
	19.208	0.023	1.038	0.027			
	19.971	0.043	0.758	0.060			1
0119−04	17.199	0.015	0.993	0.014	0.450	0.015	
	20.645	0.050	0.695	0.078	0.156	0.324	2
0122−00	16.747	0.022	0.305	0.037			
	19.771	0.037	1.369	0.057			
0220−14	18.776	0.024	0.603	0.030			
	20.314	0.050	0.980	0.064			
0225−01	18.485	0.017	0.715	0.020	0.408	0.038	
	20.033	0.037	0.853	0.053	0.615	0.145	2
0226−03	17.444	0.017	0.642	0.018			
	20.951	0.077	1.389	0.095			
0229+13	18.253	0.019	1.005	0.021	0.197	0.026	
	20.401	0.049	1.285	0.062	1.490	0.489	
0232−04	16.404	0.014	0.660	0.012			
	20.866	0.062	1.851	0.070			
0302−22	16.641	0.014	0.692	0.012	0.284	0.008	
	18.943	0.022	1.785	0.024			
	20.327	0.042	0.722	0.062	0.481	0.191	2
0329−25	17.742	0.017	0.422	0.018			
	20.238	0.042	2.345	0.043			
0335−33	18.415	0.020	1.046	0.024			
	19.260	0.031	1.547	0.034			
0347−24	17.148	0.016	0.673	0.025			
	21.221	0.057	1.997	0.067			
0438−16	17.907	0.016	0.660	0.010	−.075	0.012	
	20.116	0.036	0.602	0.052	0.279	0.099	
0448−39	16.818	0.019	0.680	0.021			
	17.443	0.021	2.714	0.022			
0451−28	17.944	0.016	0.481	0.018			
	19.921	0.036	0.862	0.052			
0636+68	16.464	0.021	0.675	0.025	0.848	0.016	
	17.147	0.022	0.675	0.027	0.542	0.023	
	19.086	0.048	0.715	0.058	0.682	0.105	2
	18.522	0.033	2.091	0.036			
0642−34	17.857	0.015	0.841	0.010	0.368	0.023	
	18.581	0.017	0.894	0.014	0.822	0.042	
	19.681	0.025	1.832	0.024			
	20.600	0.046	0.836	0.067	0.370	0.176	2
0731+65	18.125	0.017	0.432	0.029			
	19.894	0.040	1.199	0.064			
0804+49	18.205	0.040	0.693	0.049			
	20.538	0.114	2.464	0.116			
0808+28	18.094	0.025	0.727	0.027	0.234	0.009	
	20.102	0.073	0.952	0.085	0.795	0.081	
	18.599	0.029	1.147	0.030			
0827+24	17.494	0.036	0.356	0.039			
	18.098	0.041	2.131	0.043			

Table 2—Continued

QSO Field	V	σ	$V-I$	σ	$B-V$	σ	Comments
	20.331	0.160	1.927	0.163			
0830+11	18.010	0.080	0.380	0.082			
	20.350	0.080	1.623	0.088			
0831+10	19.261	0.068	0.729	0.091			
	19.272	0.059	2.073	0.067			
0848+16	17.542	0.040	0.655	0.051			
	19.265	0.111	2.325	0.115			
0903+17	17.985	0.045	1.141	0.055			
	19.803	0.112	2.278	0.118			
0932+36	18.703	0.031	0.614	0.037			
	20.498	0.120	1.218	0.135			
1008+13	16.370	0.027	0.561	0.038			
	17.116	0.030	1.475	0.039			
1011+09	17.649	0.043	1.285	0.051			
	19.471	0.057	0.040	0.116			
1038+06	16.449	0.027	0.392	0.036			
	17.370	0.032	1.961	0.039			
1148+38	17.125	0.014	0.636	0.005	0.325	0.007	
	20.341	0.070	0.760	0.081	0.527	0.101	2
	20.993	0.115	2.588	0.116			
1211+33	17.451	0.026	0.657	0.034	0.152	0.013	
	18.780	0.057	0.678	0.079	0.649	0.033	3
	19.739	0.125	0.717	0.170	0.649	0.033	3
1248+40	16.235	0.021	0.430	0.026			
	20.507	0.102	1.708	0.109			
1309+34	17.581	0.029	0.530	0.029			
	21.190	0.110	1.209	0.136			
	19.850	0.064	2.697	0.064			
1323+65	17.356	0.025	0.603	0.036			
	18.479	0.038	1.114	0.049			
2251+24	18.176	0.019	1.006	0.021	0.722	0.032	
	18.588	0.021	1.512	0.022			
	19.375	0.028	1.311	0.036	1.581	0.142	
2345+06	18.417	0.018	0.812	0.022			
	19.777	0.029	1.970	0.036			
2353+15	18.034	0.018	0.801	0.029			
	19.730	0.033	1.425	0.046			

Note. — First line for every field gives results for quasar, following lines are for stars in the field fainter than the quasar. Positions of the stars are given in Gould et al. (1993).

1- Not a lensed image, based on absence of radio emission, see text and Maoz et al. (1993a).

2- Star, based on spectroscopy with the MMT.

3- $1''$-separation binary, see Gould et al. (1995). $B-V$ color is for the combined pair.

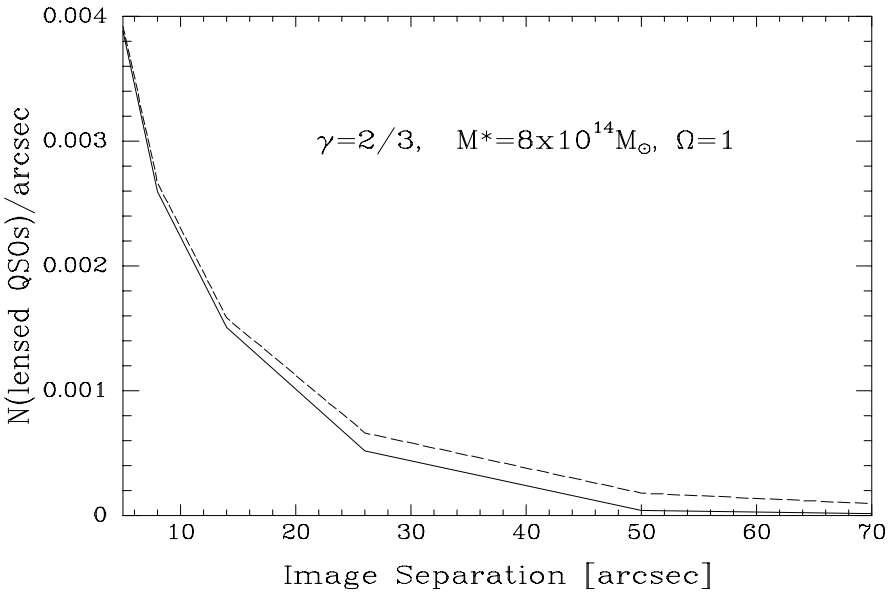

Fig. 1.— The expected distribution of lensed quasars for a particular choice of parameters. γ is the power law index relating cluster scale length and mass. M^* is the exponential cutoff mass in the cluster mass function, here assumed to have a value 4 times the Bahcall & Cen (1993) estimate. Dashed line is the distribution that would result if the angular selection function resulting from the positioning of the quasar on the detector did not exist. The total number of expected lensed quasars with separation $> 7''$ in this particular model is 0.032 (0.041 without the angular selection function), consistent with our null result.

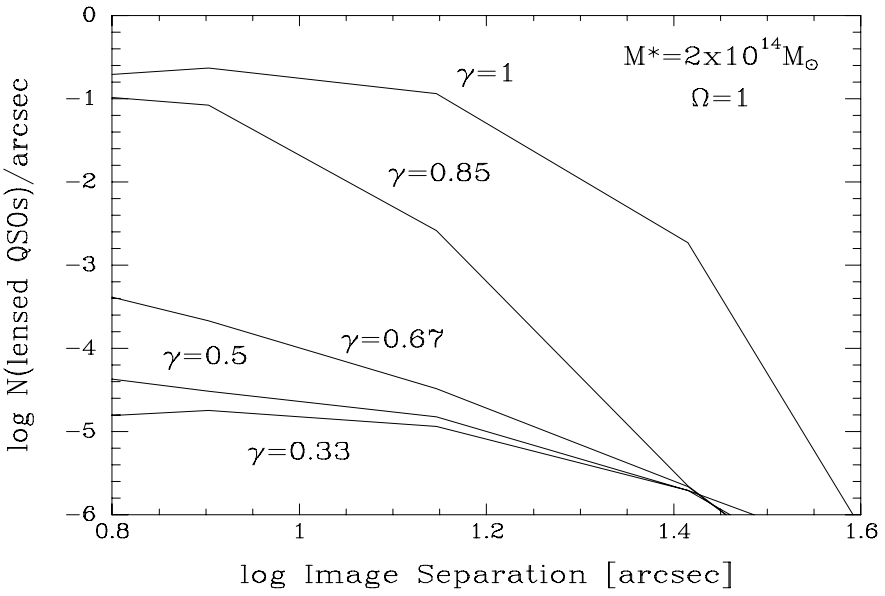

Fig. 2.— The expected number of lensed quasars for various values of γ, shown on a logarithmic scale. The models with $\gamma \lesssim 0.7$ produce $<< 1$ lensed quasars in our sample, and are therefore consistent with our observed null result, even if the other input parameters, such as the number density of clusters or the mass of a an M^* cluster have both been underestimated by an order of magnitude.

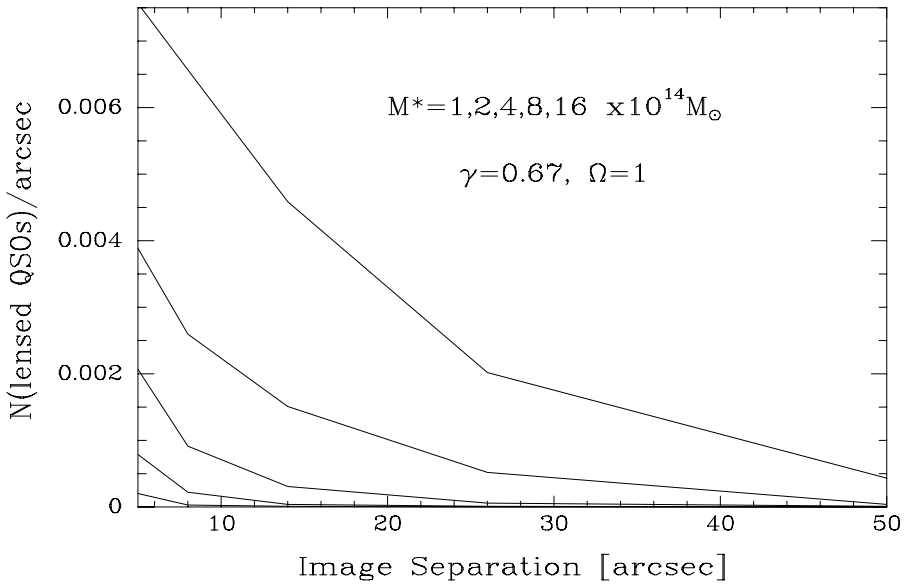

Fig. 3.— The dependence of the lensing distribution on M^*, the cutoff mass in the cluster mass function. The higher curves have higher M^*; the second curve from the bottom corresponds to the Bahcall & Cen (1993) value. For low γ, such as assumed in this example ($\gamma = 2/3$), the total number and the mean image separation of lensed quasars both increase with M^*.

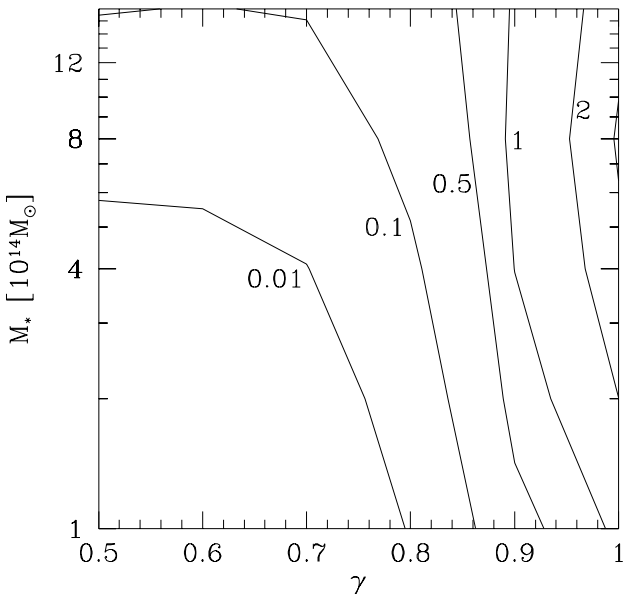

Fig. 4.— Total number of lensed quasars with $> 7''$ separation expected for combinations of γ, the index of the power-law relating cluster scale length to mass, and M^*, the cutoff mass in the cluster mass function. The Bahcall & Cen (1993) value for M^* is $2 \times 10^{14} h^{-1} M_\odot$. $\Omega = 1$ is assumed; lowering Ω to 0 approximately doubles the predicted number of lensed quasars. Models predicting ≥ 3 (≥ 4.5) lenses can be rejected at 95% (99%) confidence.

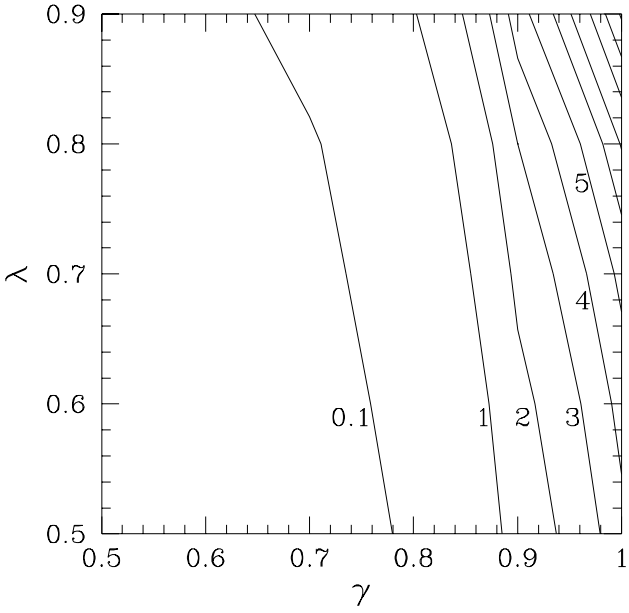

Fig. 5.— Same as fig. 4, but for combinations of γ and λ, the cosmological constant in dimensionless form, for flat ($\Omega + \lambda = 1$) cosmologies. High-λ models in which low-mass clusters have large central mass concentration (i.e., high γ) produce several large-separation lenses, and can be rejected.

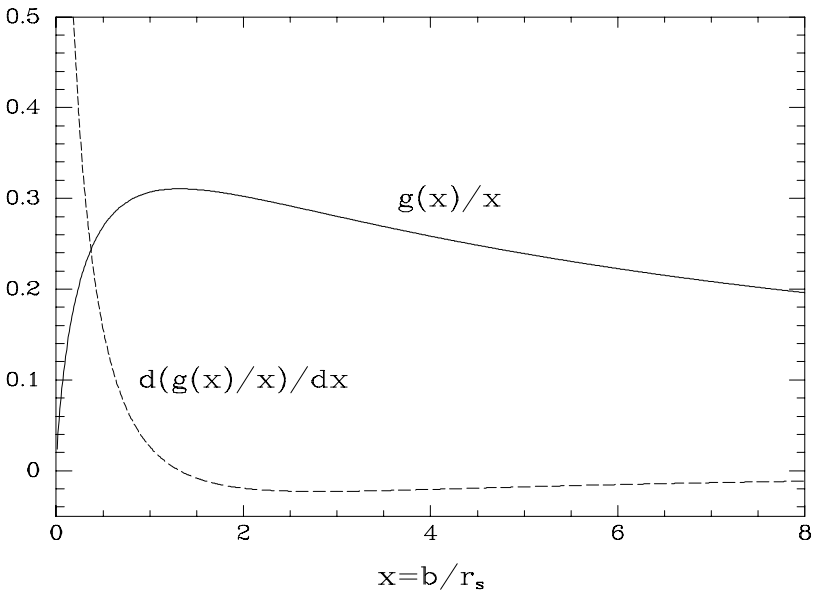

Fig. A1.— The dimensionless function $g(x)/x$ which characterizes the bending angle of a light ray passing at impact parameter x from a cluster with a Navarro, Frenk, & White profile (eqs. A5–A8). The dashed line is this function's derivative.